Remote sensing of the cyanobacteria life cycle: A mesocosm temporal assessment of a *Microcystis* sp. bloom using coincident unmanned aircraft system (UAS) hyperspectral imagery and ground sampling efforts

Kaytee Pokrzywinski [a,b,#,*], Richard Johansen [b,#,1], Molly Reif [b,c], Scott Bourne [b], Shea Hammond [b], Brianna Fernando [b]

[a] *National Oceanic and Atmospheric Administration, National Centers for Coastal Ocean Science, 101 Pivers Island Rd, NC, 28516 United States*
[b] *Environmental Laboratory, US Army Engineer Research and Development Center, 3909 Halls Ferry Rd, Vicksburg, MS United States*
[c] *Joint Airborne Lidar Bathymetry Technical Center of Expertise, 7225 Stennis Airport Rd, Kiln, MS United States*

ARTICLE INFO

ABSTRACT

Remote sensing technologies offer a consistent, spatiotemporal approach to assess water quality, which includes the detection, monitoring, and forecasting of cyanobacteria harmful algal blooms. In this study, a series of *ex-situ* mesoscale experiments were conducted to first develop and then monitor a *Microcystis* sp. bloom using a hyperspectral sensor mounted on an unmanned aircraft system (UAS) along with coincident ground sampling efforts including laboratory analyses and *in-situ* field probes. This approach allowed for the simultaneous evaluation of both bloom physiology (algal growth stages/life cycle) and data collection method on the performance of a suite of 41 spectrally-derived water quality algorithms across three water quality indicators (chlorophyll *a*, phycocyanin and turbidity) in a controlled environment. Results indicated a strong agreement between Lab and Field-based methods for all water quality indicators independent of growth phase, with regression R^2-values above 0.73 for mean absolute percentage error (MAPE) and 0.87 for algorithm R^2 values. Three of the 41 algorithms evaluated met predetermined performance criteria (MAPE and algorithm R^2 values); however, in general, algal growth phase had a substantial impact on algorithm performance, especially those with blue and violet wave bands. This study highlights the importance of co-validating sensor technologies with appropriate ground monitoring methods to gain foundational knowledge before deploying new technologies in large-scale field efforts.

1. Introduction

Harmful algal blooms (HABs) are defined as any quantity of phytoplankton that negatively contribute to aquatic ecosystems, for example through the release of toxins or resulting hypoxia associated with algal cell death. Freshwater HABs are typically dominated by cyanobacteria, commonly referred to as blue-green algae, which are known to have lasting adverse impacts on water quality and ecosystem services, including shading and subsequent degradation of submerged aquatic vegetation, changes to aquatic food webs, rapid decreases in dissolved oxygen levels (hypoxia) that drive fish kills, and prolonged hypoxia that could impact benthic macro-invertebrate communities (Havens, 2008;

Paerl et al., 2001). Cyanobacteria HABs (cyanoHABs) are most notably known for their production of potent toxins that can sicken or kill humans and wildlife (Graham, 2006; Linkov, et al. 2009). However, monitoring at-risk water bodies remains a challenge as *in-situ* and grab sampling efforts are time-intensive and costly, and also only provide information at discrete locations in space and time. Therefore, this approach may not accurately reflect conditions across an entire waterbody and ultimately limit the ability to confidently utilize this information for early detection, prevention, and mitigation strategies. Fortunately, remote sensing technology offers a consistent approach to assess water quality at the local level, while being relevant at the regional and even national scale (Kloiber et al., 2002; Ritchie et al.,

2003), improving monitoring capabilities and increasing situational awareness for early bloom detection. Remote sensing approaches can be used to help prioritize and improve *in-situ* and ground monitoring efforts for greater field efficiencies, while at the same time ground efforts can increase our understanding of geospatial tools and be used to validate remote sensing methods (Beck et al., 2019; Beck et al., 2017; Beck et al., 2016).

There are two primary optically-based ground monitoring strategies that can be used to estimate relative biomass concentrations which capitalize on the natural process of photosynthesis within algae, including absorbance and fluorescence (MacIntyre and Cullen, 2005; Wood et al., 2005). In photosynthesis, light can be utilized in two ways: 1) it can be absorbed/consumed for metabolic energy, or 2) it can be used in non-photochemical quenching, in which excess radiation energy can be harmlessly released as either heat or light (fluorescence) (reviewed in Maxwell and Johnson, 2000; Ni et al., 2019). In absorbance measurements, a concentration is measured as light attenuates through a sample. Absorbance readings are primarily products of absorption, reflection, and scattering of light while passing through the medium (Gustavs et al., 2009). In fluorescence measurements, an excitation light is used to saturate chlorophyll *a* or phycocyanin molecules at specific wavelengths (reviewed in Maxwell and Johnson, 2000). Following excitation, released light from pigment relaxation is measured, typically at a lower energy (i.e. higher wavelength), to estimate biomass and physiological health of algae (MacIntyre and Cullen, 2005). During times of stress, light absorption can become uncoupled with metabolism and result in greater non-photochemical quenching, i.e. higher fluorescence values (discussed in Maxwell and Johnson, 2000). However, fluorescence measures have still been shown to corroborate biomass estimates during active growth stages (MacIntyre and Cullen, 2005; Pokrzywinski et al., 2012; Takahashi, 2019; Wood et al., 2005). Furthermore, under field conditions, the fluorescence output exhibits a wider dynamic range than the corresponding absorbance signal. As such, many field instruments utilize optical fluorescence techniques to provide a relative quantification of algal biomass.

Key ground sampling monitoring strategies include the algal biomass indicators chlorophyll *a* and phycocyanin, and indirectly turbidity. Chlorophyll *a* and phycocyanin are pigments specifically found in cyanobacteria that are naturally fluorescent molecules, and thus, are commonly measured using fluorescence (but can be measured using absorbance), whereas turbidity is measured directly using light scattering (nephelometry) or indirectly using absorbance. Various *in-situ* sensors and laboratory techniques call upon different excitation wavelengths and emission wavebands for phytoplankton fluorescence-based detection strategies. In contrast, turbidity is an estimate of water clarity that may include algal cells, inorganic sediments or any other particles that scatter light. Light scattering (nephelometry) and absorbance wavelengths for turbidity also vary, which may have the potential to influence biomass estimations when using different instrumentation in the laboratory or field.

In addition to laboratory and field-based methods, passive remote sensors can also be used to assess water quality by measuring reflected light energy or solar radiation emitted from the water surface and upper portion of the photic zone across specific wavelengths of the electromagnetic spectrum. As such, algorithm development has resulted in successful detection and quantification of cyanoHAB pigments (chlorophyll *a*, phycocyanin) and water quality indicators associated with blooms, primarily turbidity (Beck et al., 2016; Johansen et al., 2019; Mishra et al., 2019; Mishra and Mishra, 2014; Randolph et al., 2008; Simis et al., 2005; Stumpf et al., 2016; Wynne et al., 2008); yet, most algorithms have been developed for multispectral satellite sensors (e.g. Ocean Land Color Imager [OLCI] on Sentinel-3, Medium-Spectral Resolution Imaging Spectrometer [MERIS], etc.) and tend to be locally optimized for a particular study area, temporal or seasonal period, water quality indicator, and sensor band configuration. The portability of satellite-derived algorithms as applied to imagery with higher spectral

(hyperspectral), spatial, and temporal resolutions is not well understood particularly with respect to assessing the life cycle characteristics of cyanobacteria bloom events. For example, hyperspectral sensors have greater utility for detecting and quantifying HAB indicators as they have hundreds of narrow spectral bands which allows for the identification of spectral features characteristic of HABs: green reflectance (550 nm), phycocyanin absorption (620 nm), chlorophyll *a* absorption (665 nm - 680 nm), and cell backscattering or turbidity (709 nm) (Davis and Bissett, 2007; Lekki et al., 2019; Shen et al., 2012; Stumpf et al., 2016).

Complementary to the advancements in sensors, Unmanned Aircraft System (UAS) technology is also rapidly evolving and continually being explored to reveal new applications, including water quality monitoring (Cillero Castro et al., 2020). As such, UAS technology has the ability to help overcome some of the limitations associated with traditional satellite remote sensing, such as operational flexibility to conduct frequent (minutes to days) surveys during ideal weather conditions coincident with developing bloom events. Furthermore, although spatial coverage is limited in UAS-based approaches compared to satellite platforms, increased spatial resolutions associated with UAS sensors affords a greater ability to frequently monitor small waterbody systems. Currently, there are no commercial UAS sensors specifically designed for cyanoHAB detection and monitoring, with most designed for precision agriculture or terrestrial applications (Cillero Castro et al., 2020). However, the combined advantages of a UAS platform (e.g., operation flexibility, lower flying altitude for increased spatial resolution) with a hyperspectral sensor (e.g., higher spectral resolution) offer a unique and highly specific means to explore cyanoHAB detection and bloom dynamics or characteristics that may not be possible with current satellite-based sensor-platform combinations. Thus, the technology may help to develop early detection approaches and bridge the gap between traditional field and remote sensing approaches.

The overall goal of this study was to evaluate and compare a suite of sensing methods to assess detection capabilities and life cycle trends of a cyanoHAB bloom in a controlled environment. More specifically, the primary objectives included the following: 1) synthesize a *Microcystis* sp. bloom event in *ex-situ* mesocosms, 2) monitor bloom development by conducting a multi-method, temporal experiment, including laboratory analyses (grab samples), *in-situ* field probes, and UAS hyperspectral imaging to measure or estimate HAB water quality indicators (chlorophyll *a*, phycocyanin and turbidity), 3) compare water quality results across analytical methods (both within and between indicators) and bloom physiological state (algal growth stages/life cycle), and 4) assess the performance and life cycle consistency of spectrally-derived algorithms applied to UAS hyperspectral imagery. This work will help with the future development and utility of using UAS hyperspectral systems and ground sampling approaches for bloom monitoring to build consistency and portability of methods across space and time. Furthermore, this work highlights the importance of understanding what is measured (cyanoHAB indicator), how it is measured (method), and when it is measured (algal physiological state), as all of these factors have implications for monitoring performance and mitigation strategies.

2. Methods

2.1. Experimental Design

Approximately 4 L of natural cyanobacteria bloom sample dominated by *Microcystis* sp. was obtained from Milford Reservoir in Kansas (39°05′ N, 96°54′ W). The natural bloom was cultivated in 50 L glass aquaria inside an environmental growth chamber (12 total) at 23°C for 2 weeks to increase the density prior to outdoor mesocosm tank inoculation. The bloom sample was cultured in reverse osmosis (RO) water enriched with nitrate, phosphate, magnesium and calcium salts, iron (+EDTA), and trace metals at BG-11 concentrations (Andersen, 2005) with the exception of decreased nitrate at 0.15 g•L^{-1}, one-tenth of the standard BG-11 concentration (BG-11/low N). A lower nitrate supply

was used based on laboratory studies that showed strong bloom development and subsequent senescence at this concentration after 10 days of growth (data not shown). A low supply of air was injected into the aquaria to increase dissolved oxygen concentrations and promote general mixing to stimulate phytoplankton productivity.

Following indoor cultivation, the contents of each 50 L glass aquaria were transferred to 4 outdoor mesocosm tanks containing either 1100 (1.5 m x 2.25 m) or 1900 L (2.25 m diameter) (2 each) of media on 03 August 2017, along-side two reference tanks (one each at 1100 and 1900 liters) with blank BG-11/low N for each mesocosm tank type (Fig. 1). Mesocosm tanks that received algae were all started at an optical density of 0.02 at 680 nm (chlorophyll *a* absorbance) as determined on a UV-1800 spectrophotometer (Shimadzu, Kyoto, Japan). Throughout the study, mesocosms were still dominated by *Microcystis* sp. Note that *in situ* and grab sample data from mesocosms were obtained in coincidence (< 10 min) with UAS flyovers except on day 10 when UAS flights were not accompanied by grab/*in situ* mesocosm measurements. To ensure consistency, mesocosms were manually stirred immediately prior to all data collection timepoints. The missing mesocosm data were estimated by interpolating the mesocosm tank data for days 9 and 11.

2.2. Mesocosm Sample Collection

Approximately every other day, physical water quality indicators were collected via an EXO2 multiparameter water quality sonde (YSI, Yellow Springs, OH) including probes to monitor temperature (°C), pH (units) and dissolved oxygen (mg•L^{-1}) and grab sampling for laboratory-based analysis. Two sets of algal density measurements co-occurred for each mesocosm with algae including: 1) *in vivo* chlorophyll *a* (μg•L^{-1}), *in vivo* phycocyanin (μg•L^{-1}), and turbidity (Nephelometric Turbidity Units [NTU]) via the EXO2 sonde (YSI) and 2) *in vivo* chlorophyll *a* (Relative Fluorescence Units [RFU]) and *in vivo* phycocyanin (RFU) fluorescence from a hand-held fluorometer, AquaPen-C AP-C 100 (Photon Systems Instruments, Drazov, Czech Republic), and turbidity (Absorbance Units [AU]) from a UV-Vis 1800 spectrophotometer (Shimadzu). All EXO2 sonde probes were calibrated before the study according to the manufacturer's recommendations (YSI, 2020). The EXO2 sonde measured chlorophyll *a* excitation at 470 +/- 15 nm and phycocyanin excitation at 590 +/- 15 nm, both with emissions at 685 +/- 20 nm using *in vivo* fluorescence (RFU). For the EXO2 sonde, RFU were internally converted to concentrations (μg•L^{-1}) as determined by pre-calibration using Rhodamine dye. The AquaPen-C AP-C 100 measured chlorophyll *a* fluorescence at an excitation of 455 nm and phycocyanin fluorescence at 620 nm, both with an emission band of 667 nm to 750 nm, which was comparable to the EXO2 sonde. The EXO2 sonde measured turbidity through light scattering (nephelometry) at 860 +/- 15 nm, where the UV-Vis 1800 spectrophotometer measured

turbidity (absorbance) at 750 nm to avoid overlap with chlorophyll *a* absorbance. Thus, the method adopted in this study compared *in vivo* measurements of pigments (chlorophyll *a*, phycocyanin) through two optical techniques (absorption and fluorescence) and also compared the *in vivo* turbidity measurements based on absorption and nephelometry. For analysis the mesocosm data were split into two groups including:

1) Grab sampling data, termed Lab, consisting of measurement end-points conducted in the laboratory with the AquaPen fluorometer and spectrophotometer, and
2) *In-situ* data, termed Field, consisting of data generated from the EXO2 data sonde.

In order to ensure accurate comparison, all ground sampling measurements were acquired simultaneously with UAS flights.

2.3. Mesocosm Data Organization

For this study, mesocosm data obtained through grab samples/*in situ* measurements were split into two groups in which UAS image-derived algorithm metrics were ranked as they relate to cyanobacteria growth phase, specifically targeting active growth stages and the full life cycle. Algal/bacterial growth phases can be generically determined based on characteristic growth patterns. Typical sequential growth phases are as follows: 1) an initial period of limited/no growth (lag phase), 2) a period of consistent positive logarithmic growth (exponential phase), 3) a period of little to no growth (stationary phase), and 4) bloom demise (termination phase) completing a bloom life cycle cultivated in the presence of a limiting nutrient (Wang et al., 2015; Fig. 2). Given the availability of coincident UAS imagery and grab samples/*in situ* measurements, the data were split into the following two groups:

1) Active growth stages, termed Active Growth, consisting of data from the lag phase (day 1) and the exponential growth phases (days 7 and 10).
2) Full life cycle, termed Full Cycle, consisting of data from the lag phase (day 1), exponential (days 7 and 10), and stationary phases (day 11).

2.4. Unmanned Aircraft Hyperspectral Imagery Collection and Pre-processing

For imagery acquisition, a Multirotor G4 SkyCrane UAS (Avirtech, Singapore) flew repeatable autonomous flights at 30 m over the mesocosm tanks with a Headwall Photonics Nano-Hyperspec sensor, which has 270 spectral bands across a spectral range 400 – 1000 nm (Tbl. 1). Given that the Headwall Nano-Hyperspec sensor is a line scanner, the
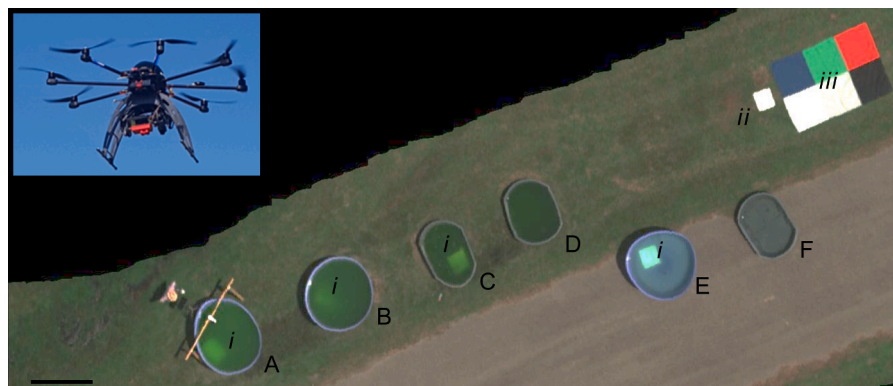

Figure 1. Aerial image of mesocosm study area and SkyCrane UAS (inset). Experimental (A-D) and reference (E-F) mesocosms (A-D) were conducted in either 1900 L (A, B, E) or 1100 L (C, D, F) tanks. White Teflon coated reference targets (i), Spectralon calibration target (ii) and a color panel (iii) were used for image calibration and visual reference. Scale bar is 2.25 m.
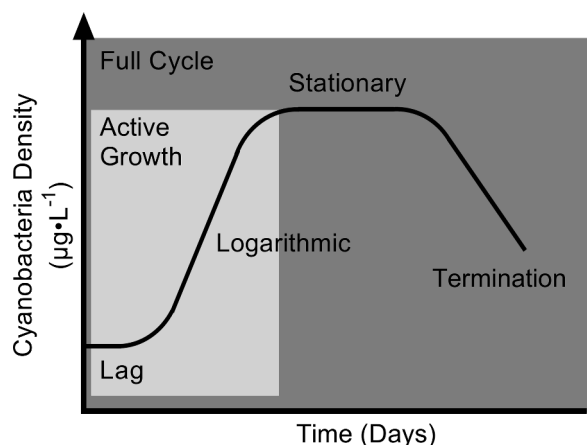
Figure 2. Conceptualization of a typical cyanobacteria life cycle in batch culture. Cyanobacteria growth over time in batch culture can be broken down by 1) a lag phase, 2) a logarithmic phase, 3) a stationary phase, and 4) a termination phase. Active Growth (light gray rectangle) is designated by phase 1 and 2 while the Full Growth Cycle (dark gray rectangle) encompasses all phases 1 through 4.

Table 1
Headwall Nano-Hyperspectral sensor specifications at 30m altitude

Platform	Multirotor G4 SkyCrane
Sensor	Headwall Photonics Nano-Hyperspec
Sensor Type	Push-broom
Payload	4.5 kg
Focal Length	12 mm
Spectral Range	400 - 1000 nm VNIR, 270 spectral bands
Spectral Resolution	2.3 nm
Spatial Resolution	~ 2.2 cm
Max Flight Time	15 minutes

frame period and altitude were used to determine the aircraft speed needed to produce square pixels as the frame period is dictated by atmospheric conditions and available light. UAS flights occurred between 04 August 2017 and 15 August 2017, and all flights occurred +/- 2 hours of solar noon and did not exceed 15 minutes in duration. Four flights produced quality imagery that also coincided with ground sampling events and algal biomass accumulation (Tbl. 2). Additionally, all flights were optimized for data collection with an image footprint side lap of 40% to ensure complete coverage of the target area. Detailed information on image system specifications and data collection can be seen in the Supplemental Materials *Section 1.1*.

The radiometric correction of the hyperspectral imagery was performed following Headwall Photonics standards in the SpectralView (version 5.5.1) software. The conversion of digital number (DN) to radiance of the Nano-Hyperspec data was conducted using radiometric calibration and Dark Reference files provided by Headwall. Following in the SpectralView software, radiance values were subsequently converted to reflectance using reference spectra obtained from a Spectralon white calibration panel sampled at 1 Hz from an Analytical Spectral Devices FieldSpec Pro FR Portable Spectroradiometer (350 nm – 2500 nm). The transformation provided measurements in physical units of

milliwatts per square centimeter per steradian (a measure of the amount of the field of view from some particular point that a given object covers) per micrometer ($mW/cm^2 \bullet sr \bullet \mu m$), thus eliminating the problem of specific measuring scales for each sensor (Hruska et al. 2012). Detailed information on image pre-processing can be seen in the Supplemental Materials *Section 1.2*.

2.5. Imagery Analysis and Algorithm Evaluation

After the imagery from each flight was pre-processed, a subset of 12 × 12 pixels (26.4 × 26.4 cm) from the center of each mesocosm was extracted from the corresponding images. This 12 × 12 pixel subset was sufficiently large to accurately represent the overall mesocosm conditions, but small enough to avoid signal contamination by adjacent issues originated from mesocosm tank edges, shadows, or other features. These extracted data were then imported and analyzed using the open-source programming language, R v.4.0.2, and the graphic user interface (GUI), RStudio v.1.3.1093 (https://www.rstudio.com/). In total there were 16 clipped and extracted reflectance values (four mesocosm tanks with algae by four sampling days) from hyperspectral images. These values were then analyzed using a modified version of the *waterquality* R package, specifically designed for the Headwall Photonics Nano-Hyperspec sensor. This script contains 41 empirically-based water quality algorithm packages that were each designed to estimate chlorophyll *a*, phycocyanin and turbidity from reflectance imagery (Johansen et al., 2019; R Core Team, 2017) (Tbl. 3). These include the following: 2-band difference algorithms (Beck et al., 2017; Mishra, et al. 2009; Schalles and Yacobi, 2000), 3-band difference algorithms (Dekker, 1993; Mishra and Mishra, 2014), 2-band subtraction algorithms (Amin et al., 2009; Beck et al., 2017), normalized difference chlorophyll *a*/cyanobacterial indices (Mishra and Mishra, 2014), and cyanobacterial indices (Wynne et al., 2008). All 41 algorithms were calculated using the original 2.3 nm spectral bands nearest to the original algorithm's band centers as possible, which made it possible to not only determine the performance of these algorithms, but also to explore how water quality indicators, algal physiology, and collection methods impact algorithm performance and accuracy (Tbl. 3).

Using statistical models, the relative algorithm index values (41 total) were then directly compared to ground observations from the mesocosms to estimate chlorophyll *a*, phycocyanin and turbidity concentrations (Stumpf et al., 2016). Specifically, a linear regression analysis was conducted between the three water quality indicators and algorithm indices, by method (Lab vs Field) and growth phase group (Active Growth vs Full Cycle). Algorithm R^2 values were generated using the *waterquality* package's *extract lm* by calculating linear regression models, making it possible to rank algorithm performance between water quality indicators and methods by growth phase/physiological state to identify inherent methodological or growth phase bias. A comparison of mesocosm analysis methods (Lab vs Field) for each water quality indicator (chlorophyll *a*, phycocyanin, and turbidity) was conducted by plotting the algorithm R^2 value for each algorithm independent of the growth phase. Additionally, a comparison of growth phase groups (Active Growth vs Full Cycle) was conducted independent of ground monitoring method for each water quality parameter.

Table 2
UAS flights used in the analysis by date.

Date	Day	Condition	Altitude (m)	Frame Period (ms)	Aircraft Speed (m$\bullet$s^{-1})	Growth Phase Analysis
08/04/2017	1	Partly cloudy	30	7	2.64	Active, Full
08/11/2017	7	Partly cloudy	30	7	2.64	Active, Full
08/14/2017	10	Partly cloudy	30	7	2.64	Active, Full
08/152017	11	Scattered clouds	30	5	3.7	Full

Table 3
Algorithm band math and associated bands from hyperspectral imagery (rounded to the nearest whole number), reported as remote sensing reflectance for each wavelength (nm).

Water Quality Algorithm	Water Quality Indicator	Nano-Hyperspec Band Calculation (Reflectance values for the wavelengths in nm)
Al10SABI	chlorophyll	$(857 - 644) / (459 + 530)$
Am092Bsub	chlorophyll	$680 - 665$
Am09KBBI	BGA/PC	$(687 - 658) / (687 + 658)$
Be162B643sub629	BGA/PC	$644 - 629$
Be162B700sub601	BGA/PC	$700 - 602$
Be162BsubPhy	BGA/PC	$716 - 615$
Be16FLHblue	chlorophyll	$530 - (644 + [459 - 644]* SS(0.384))$
Be16FLHBlueRedNIR	BGA/PC	$658 - (857 + [459 - 857] * SS(0.5))$
Be16FLHGreenRedNIR	BGA/PC	$658 - (857 + [559 - 857] * SS(0.337))$
Be16FLHVioletRedNIR	BGA/PC	$658 - (857 + [443 - 857] * SS(0.519))$
Be16FLHviolet	chlorophyll	$530 - (644 + [430 - 644] * SS(0.467))$
Be16NDPhyI	BGA/PC	$(700 - 622) / (700 + 622)$
Be16NDPhyI644over615	BGA/PC	$(644 - 615) / (644 + 615)$
Be16NDPhyI644over629	BGA/PC	$(644 - 629) / (644 + 629)$
Be16NDTIblue	chlorophyll	$(658 - 459) / (658 + 459)$
Be16NDTIviolet	chlorophyll	$(658 - 443) / (658 + 443)$
Be16Phy2BDA644sub629	BGA/PC	$644 - 629$
Da052BDA	BGA/PC	$714 / 671$
De933BDA	chlorophyll	$600 - 648 - 625$
Gi033BDA	chlorophyll	$(671^{-1} - 716^{-1}) * 756$
Go04MCI	BGA/PC	$709 - (680 + [754 - 680] * SS(0.392))$
HU103BDA	BGA/PC	$(615^{-1} - 600^{-1}) * 725$
Kn07KIVU	chlorophyll	$(459 - 644) / 530$
MI092BDA	BGA/PC	$700 - 600$
MM092BDA	BGA/PC	$725 - 600$
MM12NDCI	chlorophyll	$(716 - 687) / (716 + 687)$
MM12NDCIalt	BGA/PC	$(700 - 658) / (700 + 658)$
MM143BDAopt	BGA/PC	$(629^{-1} - 660^{-1}) * 725$
SI052BDA	BGA/PC	$709 / 620$
SM122BDA	BGA/PC	$709 / 602$
SY002BDA	BGA/PC	$651 / 624$
TurbBe16GreenPlusRedBothOverViolet	turbidity	$(558 - 658) / 443$
TurbBe16RedOverViolet	turbidity	$658 / 443$
TurbBow06RedOverGreen	turbidity	$658 / 557$
TurbChip09NIROverGreen	turbidity	$857 / 557$
TurbDox02NIRoverRed	turbidity	$857 / 658$
TurbFrohn09GreenPlusRedBothOverBlue	turbidity	$(559 - 658) / 459$
TurbHarr92NIR	turbidity	857
TurbLath91RedOverBlue	turbidity	$658 / 459$
TurbMoore80Red	turbidity	658
Wy08CI	BGA/PC	$(687 - 671 - [716 - 671] * SS(0.333))$

SS= Spectral Shape coefficient calculated as $(\lambda - \lambda^{-})/(\lambda^{+} - \lambda^{-})$
BGA/PC = Blue-Green Algae/Phycocyanin

2.6. Algorithm Ranking Criteria

High performing algorithms were down-selected and ranked based on pre-determined criteria. An initial down-selection was based on an algorithm R^2 value > 0.70. Following this, algorithms were ranked from highest to lowest by Lab/Field averaged chlorophyll a algorithm R^2 value to illustrate individual algorithm differences between growth phases. Chlorophyll a was considered the benchmark measurement method as it is a highly common water quality indicator for monitoring algae and cyanobacteria. Algorithms were ranked as follows: Set 1 indicates algorithms that had < 5% difference in algorithm R^2 values for Active Growth and the Full Cycle; Set 2 denotes algorithms with 5% ≤ 15% deviation in the mean algorithm R^2 values between growth phases; and Set 3 signifies algorithms with > 20% deviation in the average algorithm R^2 values between growth phases. Following this, the top performing algorithms were down-selected again based on a 30% threshold for mean absolute percentage error (MAPE), which is the widely-accepted retrieval accuracy expectation for chlorophyll-a with satellite remote sensing (IOCCG, 2019).

2.7. Statistical Analyses

The results included a standard type-1 linear regression model and a more robust repeated k-fold cross-validation model with the following outputs: coefficient of determination (R^2), p-value, mean absolute error (MAE), and mean absolute percentage error (MAPE). MAPE was calculated as the | Measured – Predicted | / Measured * 100. The results of the MAPE derived from the 41 individual algorithm linear regression models were then used to explore comparisons between monitoring methods (Lab vs Field) for each water quality indicator using a non-linear (least squares-straight line) regression analysis in GraphPad Prism v. 8.4.2. Slopes and y-intercepts of regression lines were compared to a hypothetical slope of one and intercept of zero using an Extra Sum of Squares F Test with 95% confidence intervals to determine if there was bias between monitoring methods. From there the top-ranking algorithms (R^2 > 0.70) were then compared between Active Growth and the Full Cycle in relation to predicted values calculated from a hypothetical line of one indicating no difference between growth phases, to determine if there were algorithms that represented both growth phases well. Algorithms were considered to be representative of both growth phases if the error between the measured algorithm R^2 or MAPE deviated ≤ 15% from the predicted value. All significance (α) levels were set to 0.05.

3. Results

3.1. Ground Sampling Results

3.1.1. Bloom Indicators
Algal biomass indicators as determined by chlorophyll a and phycocyanin indicated good bloom development by day 11 of the study (Fig. 3). A lag period of 5 days was observed in all biomass indicators (chlorophyll a, phycocyanin, and turbidity), followed by a 4-5 day logarithmic phase (days 5-10) and senescence at days 10-11 (Fig. 3). No bloom demise was observed when the study was terminated on day 11 due to weather events. The laboratory analyses (Lab: Fig. 3A, C, E) and EXO2 sonde (Field: Fig. 3B, D, F) data showed similar trends in bloom progression. Specifically, for chlorophyll a, in the Lab method biomass was initially reported at 127 RFUs and progressed to 771 RFUs on day 11. In the Field method, chlorophyll a biomass was below the limit of detection and climbed to 187 µg•L^{-1} by day 11. For phycocyanin, the Lab method starting concentration was reported at 139 RFUs, peaking at 5,180 RFUs by day 11. For the Field method, reported phycocyanin starting concentrations were below the limit of detection and rose to 13,374 µg•L^{-1} by day 11. Turbidity measurements displayed a slightly different trend in their growth curves. Where in the Lab method, turbidity had a starting average of 0.0095 AU and peaked on day 9 at 0.1025 AU, after which it declined to an average of 0.078 AU. In the Field method, the starting average turbidity was 2.8 NTU, also peaking on day 9 at 58 NTU and declining thereafter to 27 NTU on day 11. Increased variability between mesocosm tanks was observed during later growth stages independent of indicator or method type (Fig. 3). As expected, chlorophyll a and phycocyanin indicators had more similar
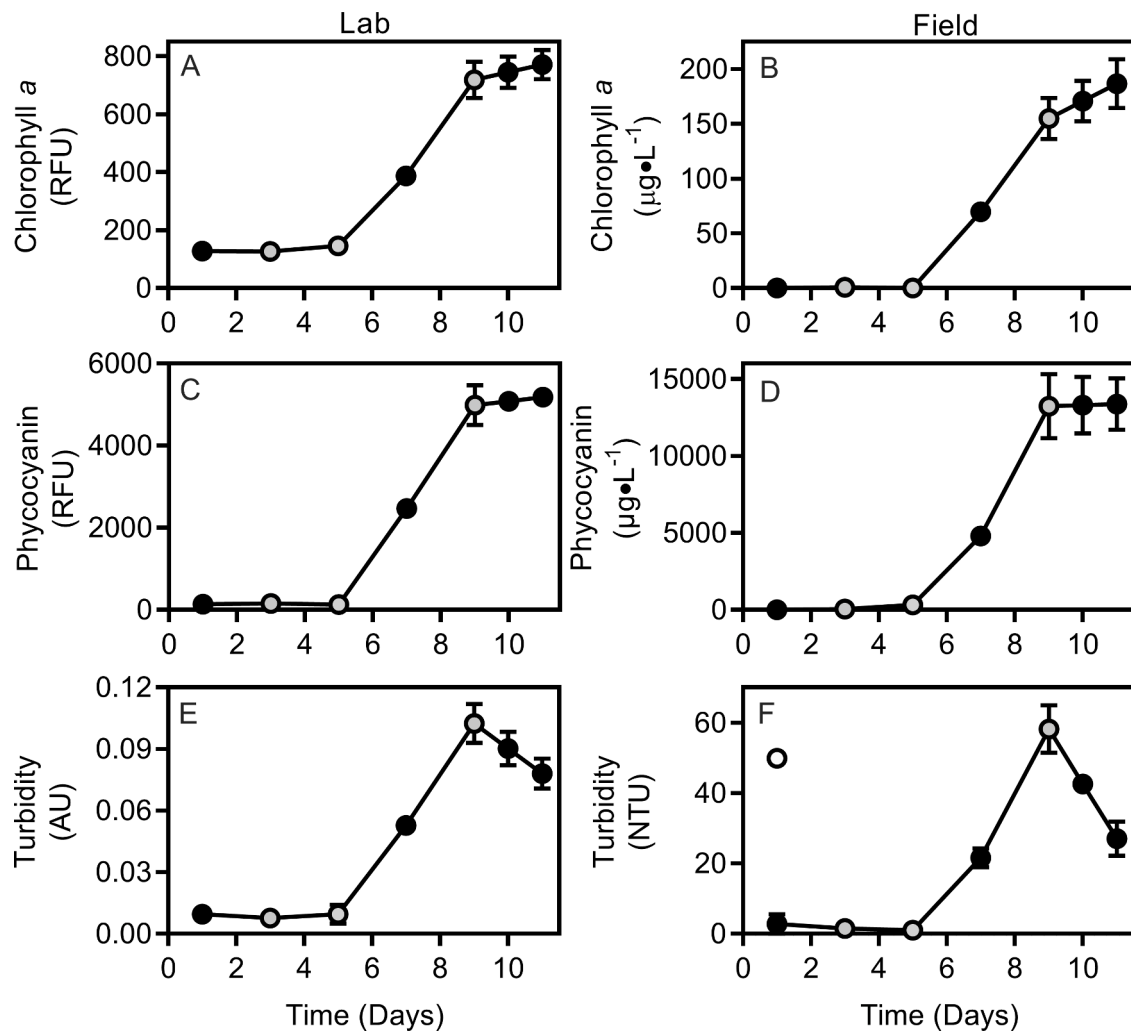
Figure 3. Average phytoplankton growth indicators chlorophyll *a* (units: relative fluorescence units: RFU; $\mu g \bullet L^{-1}$) (A-B), phycocyanin (units: RFU, $\mu g \bullet L^{-1}$) (C-D) and turbidity (units: absorbance units: AU; nephelometric turbidity units: NTU) (E-F) for Lab (A, C, E) and Field (B, D, F) methods. Circles represent the mean (n=4) concentration over time. Black symbols signify data used in the regression analysis with corresponding imagery. Open symbols in F identify outliers. Error bars denote the standard error of the mean (SEM).

growth patterns while turbidity showed greater reductions in growth during bloom senescence.

Stumpf et al., 2016).

3.2. Unmanned Aircraft Hyperspectral Imaging System

The UAS mission successfully captured coincident hyperspectral imagery for four dates encompassing the desired window within the algal bloom life cycle, allowing for temporal coverage of the bloom event. Day 1 of the experiment was the first hyperspectral image used in the algorithm analysis and had the lowest concentrations of water quality indicators during the study. As expected, there was a significant impact on the spectral signature as the algal biomass increased in intensity. Initially (day 1), the hyperspectral imagery displayed relatively high reflectance values across all wavelengths, which was likely caused by the background scattering of the mesocosm tank itself, but as the bloom intensified (days 7-11) distinct spectral features of the cyanoHAB began to emerge (Fig. 4). The most notable changes to the spectral signature occurred between approximately 500-600 nm, relating to a reflectance peak in the green spectral bands (~550 nm). Another notable feature was observed between 645-730 nm which corresponds to the prominent chlorophyll *a* absorption feature (~665-685 nm). Lastly, a third reflectance peak was observed that was linked to algal cell backscattering (~700-715 nm) (Lekki et al., 2019; Shen et al., 2012;

3.3. Methodological Comparisons

There was moderate to strong agreement between mean absolute percentage errors (MAPEs) by data collection methods (Lab vs Field), for all three indicators across all 41 algorithms independent of growth phase with R^2-values of 0.99, 0.97, and 0.70 for chlorophyll *a*, phycocyanin, and turbidity, respectively (Fig. 5, Tbl. 4). Furthermore, there was a significant difference between the slope of the regression line and a hypothetical line with slope of one (indicative of no bias between measurement methods) for both chlorophyll *a* (slope: 1.33, $p < 0.0001$) and turbidity (slope: 0.803, $p < 0.01$) but not for phycocyanin (slope: 0.969, $p = 0.11$) (Tbl. 4). This can be observed through the 95% confidence intervals (CIs) where phycocyanin is the only parameter to encompass a slope of one within the CI ranging from 0.930 to 1.01. Collectively, this suggests that there was statistical bias in algorithm errors between methods for chlorophyll *a* and turbidity. Furthermore, for phycocyanin, there was a significant difference in the y-intercept with respect to the hypothetical line with a y-intercept of zero (y-intercept: 12.55, 95% CI: 10.89 to 14.20, $p < 0.0001$), indicating that a consistent bias between Lab and Field methods may exist for this water quality indicator (Fig. 5).
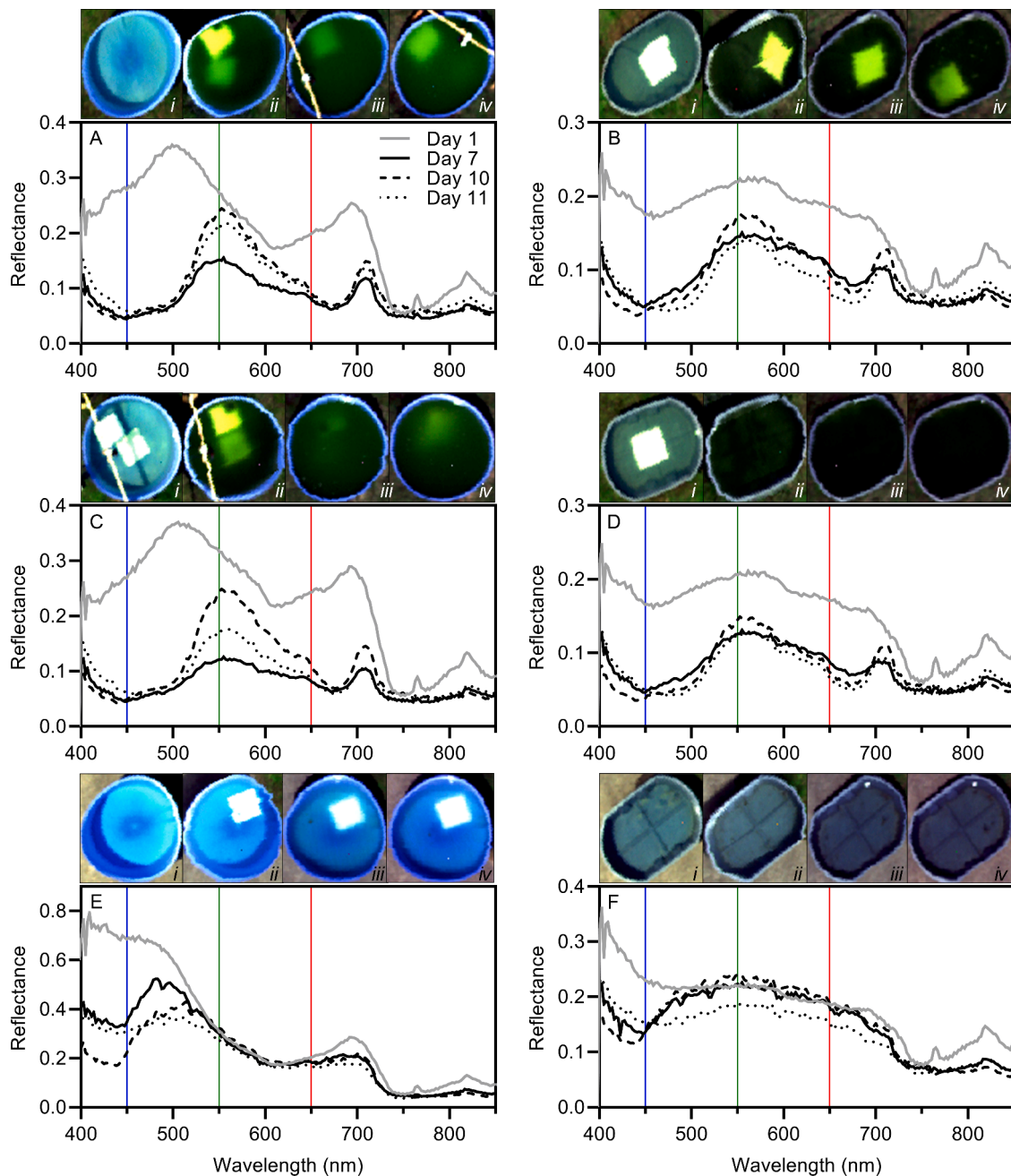
Figure 4. Time series imagery from each mesocosm collected by the Headwall UAS hyperspectral sensor. Average hyperspectral reflectance signatures of 12×12 pixel samples from days 0 (light gray), 7 (solid black), 10 (dashed black), and 11 (dotted black) for each experimental (A-D) and reference mesocosm (E-F) with red, green, and blue vertical lines corresponding to the respective wavelengths. (A-F). Insets: true (RGB) color imagery from experiment day 1 (*i*), day 7 (*ii*), day 10 (*iii*), and day 11 (*iv*) for independent mesocosms.

There was also strong agreement between algorithm R^2 values by measurement method (Lab vs Field) for all three indicators across all algorithms, independent of growth phase, having regression R^2 values of 1.0, 0.94, and 0.86 for chlorophyll *a*, phycocyanin, and turbidity, respectively (Fig. 5, Tbl. 4). Individual algorithm R^2 values ranged from approximately 0.0 to 0.95 for all water quality algorithms and growth phases, indicating that some algorithms were better at predicting water quality indicator concentrations than others (Fig. 5). Furthermore, the slopes for all water quality parameters were statistically significantly less than the theoretical slope of one ranging from 0.857 to 0.967 ($p < 0.001$) (Tbl. 4), indicating potential bias between measurement methods for each water quality indicator. However, there were high regression R^2 values ranging from 0.86 to 1.0 indicating good agreement between

methods. Furthermore, the slope of each regression line deviated from one by 3% - 14% signifying comparable algorithm performance results between each method across the algorithms tested.

Algorithm MAPE and R^2 value results suggest that there is good agreement between Lab and Field methods across all parameters independent of growth phase but that minor biases may exist between these specific methods, independent of growth phase, that may warrant further exploration to determine their impact on downstream analyses. For this study, MAPEs and R^2 values were consistent for chlorophyll *a* and phycocyanin but were more variable for turbidity, which is specifically linked to growth phase (Fig. 5). Therefore, data from both the Lab and Field methods were down-selected and averaged for further analyses. The initial down selection criteria were determined as having an
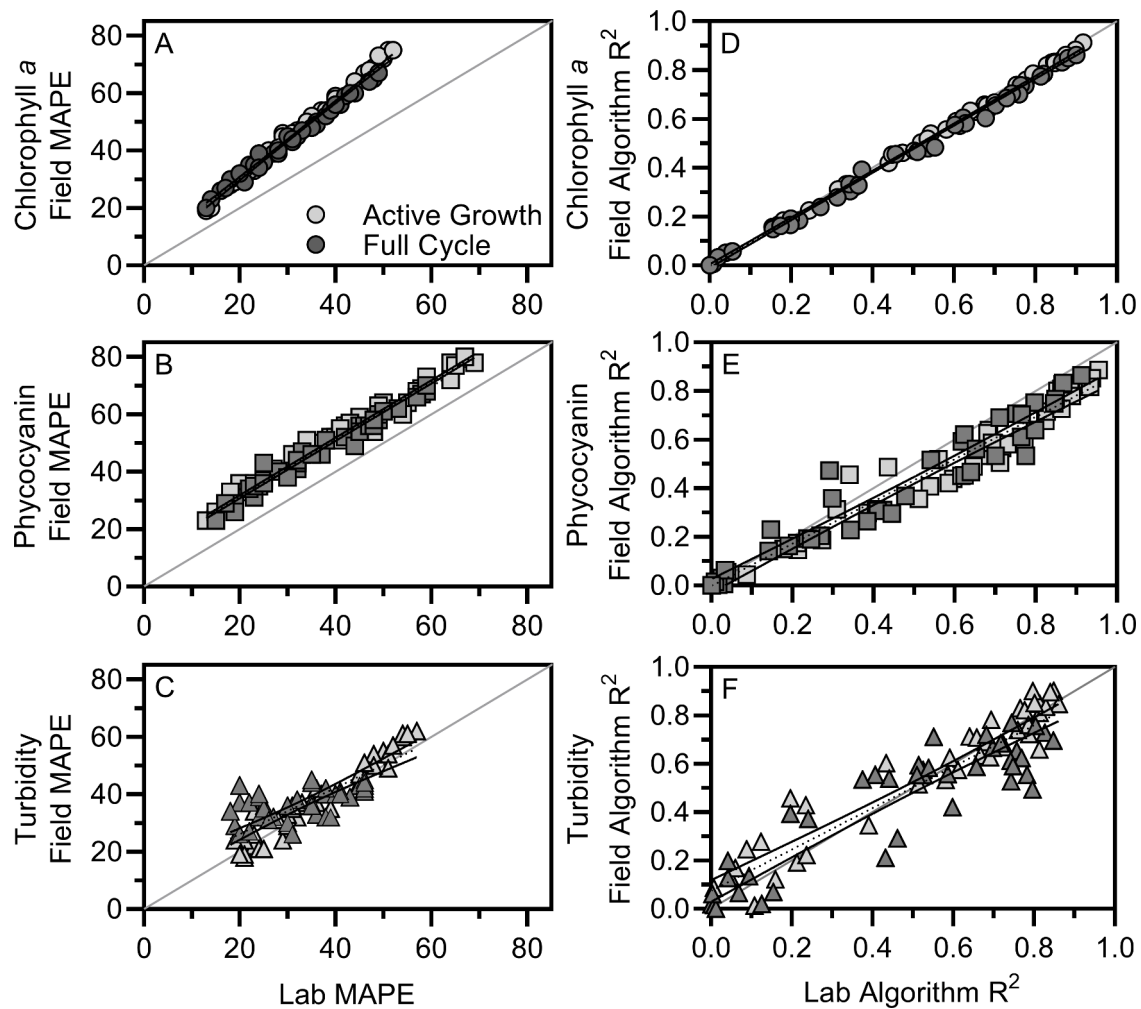
Figure 5. Comparison of algorithm performance metrics for Lab and Field methods by water quality indicator independent of growth phase. Algorithm performance was assessed as algorithm error (A-C) and R^2 values (D-F) for chlorophyll *a* (A and D, circles), phycocyanin (B and E, squares), and turbidity (C and F, triangles). Points denote mean absolute percentage error (MAPE) as determined from model performance (A-C) or R^2 values (D-F) for each algorithm and water quality indicator. Points are broken down into Active Growth (light gray) and Full Cycle (dark gray) for visualization. Black lines represent linear regression analysis (dashed) with 95% confidence intervals (solid). The gray line represents a theoretical line with a slope of one.

Table 4
Linear regression statistics for the slope between Lab and Field sensors for each water quality indicator based on MAPE and algorithm R^2 value for each algorithm.

	Mean Absolute Percent Error (MAPE)				Algorithm R^2 Value			
	Slope	95% CI	R^2	p-value Lab vs Field	Slope	95% CI	R^2	p-value Lab vs Field
Chlorophyll *a*	1.33	1.30-1.37	0.99	< 0.0001	0.967	0.953-0.980	1.0	< 0.0001
Phycocyanin	0.969	0.930-1.01	0.97	0.11	0.870	0.822-0.919	0.94	< 0.0001
Turbidity	0.803	0.687-0.920	0.70	< 0.01	0.857	0.780-0.934	0.86	< 0.001

*CI = Confidence Interval

averaged algorithm R^2 value above 0.70 in at least one condition across water quality indicators broken down by growth phase which coincided with MAPEs of ≤ 55%. Regressions with raw Lab and Field data can be seen for the high performing algorithms in Fig. 6 and Supplemental Figs. 1-9. Additionally, model outputs for all 41 algorithms can be seen in Supplemental Tbls. 1-6.

3.4. Growth Phase Comparisons

Of the 41 algorithms evaluated across each water quality indicator, 19 had at least one algorithm R^2 value > 0.70 for at least one growth phase and water quality indicator. For these high performing

algorithms, to evaluate error as a function of growth phase, the MAPEs of the combined Lab and Field data were compared for Active Growth and Full Cycle groups to a hypothetical line with a slope of one, indicative of no difference in algorithm error by growth phase. While there was a great deal of variability in MAPEs between growth phases, several algorithms had ≤ 15% deviation from predicted hypothetical values indicating good representation of both growth phases. For chlorophyll *a*, six algorithms represented both growth phases well with deviations ranging from 0%-14%, compared to five algorithms for phycocyanin with deviations ranging from 0%-12%, and 11 algorithms for turbidity with deviations ranging from 0%-12% (Fig. 7). Furthermore, the remaining algorithms had substantial bias between growth phases with
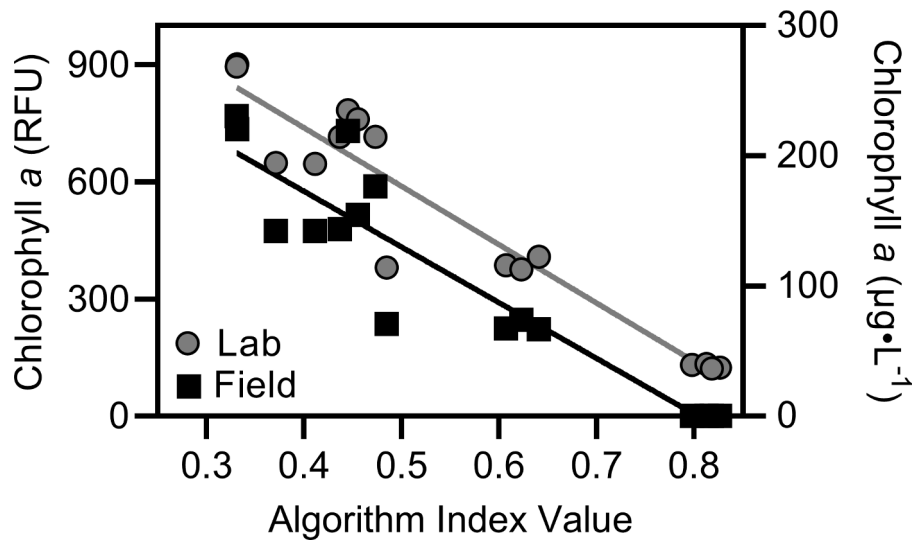
Figure 6. Representative comparison between algorithm index values and chlorophyll *a* measurements for the Full Cycle. Points denote chlorophyll *a* concentrations (μg•L^{-1}) from the Lab (gray circles) and Field (black squares) measurements for each index value for the TurbBow06RedOverGreen algorithm. Lines represent linear regression analysis for Lab (gray) and Field (black) data.
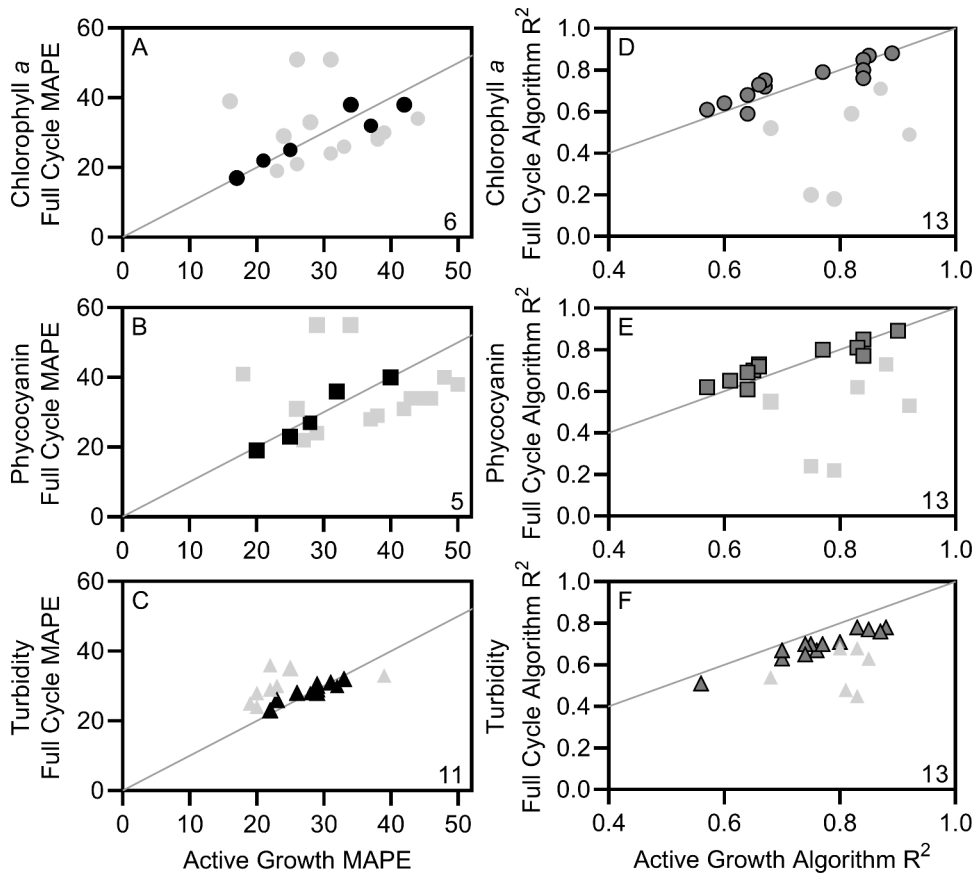

Figure 7. Comparison of algorithm performance metrics for Active Growth and Full Cycle groups by water quality indicator. Algorithm performance was assessed as algorithm error (A-C) and R^2 values (D-F) for chlorophyll *a* (A and D, circles), phycocyanin (B and E, squares), and turbidity (C and F, triangles). Points denote Lab/Field averaged mean absolute percentage error (MAPE) (A-C) or R^2 values (D-F) for each algorithm and water quality indicator that deviated from predicted values calculated from the hypothetical line by > 15% (light gray) or ≤ 15% (black for MAPEs and dark gray for R^2 values). The gray line represents a theoretical line with a slope of one, indicative of no difference between growth phases.

deviations up to 84%, 78%, and 48% for chlorophyll *a*, phycocyanin, and turbidity, respectively. These deviations were represented by higher measured MAPEs in the Full Cycle, as seen by greater variability in points above the hypothetical line (Fig. 7).

Algorithm R^2 values were also used to assess model fit as a function of growth phase for the high performing algorithms identified in *Section 3.3*. For these top-ranking algorithms, the algorithm R^2 values of the combined Lab and Field data were compared for Active Growth and Full

Cycle groups to a hypothetical line with a slope of one, again indicating no difference in algorithm R^2 values between growth phases. While there was a great deal of variability between growth phases for several algorithms, 13 out of 19 had ≤ 15% deviation from predicted hypothetical values indicating good representation of both growth phases across all water quality indicators with deviations ranging from 1%-12% for chlorophyll *a*, 1%-10% for phycocyanin, and 4%-14% for turbidity. The remaining 7 algorithms had deviations up to 125%, 114%, and 59%

for chlorophyll *a*, phycocyanin, and turbidity, respectively. These deviations were represented by lower measured algorithm R^2 values in the Full Cycle, as seen by greater variability in points below the hypothetical line (Fig. 7). Based on these findings, a closer look at individual algorithms has the potential to reveal a select group of algorithms that work well across growth phases and water quality indicators for both metrics: MAPE and R^2.

3.5. Algorithm Assessment

In Set 1 there were five algorithms that had < 5% difference in algorithm R^2 values by growth phase for chlorophyll *a* and phycocyanin (Fig. 8), and all displayed algorithm R^2 values above 0.70 (Set 1). The top three performing algorithms were: TurbBow06RedOverGreen, Da052BDA, and Be16NDPhyl644over615, all having < 2% deviations
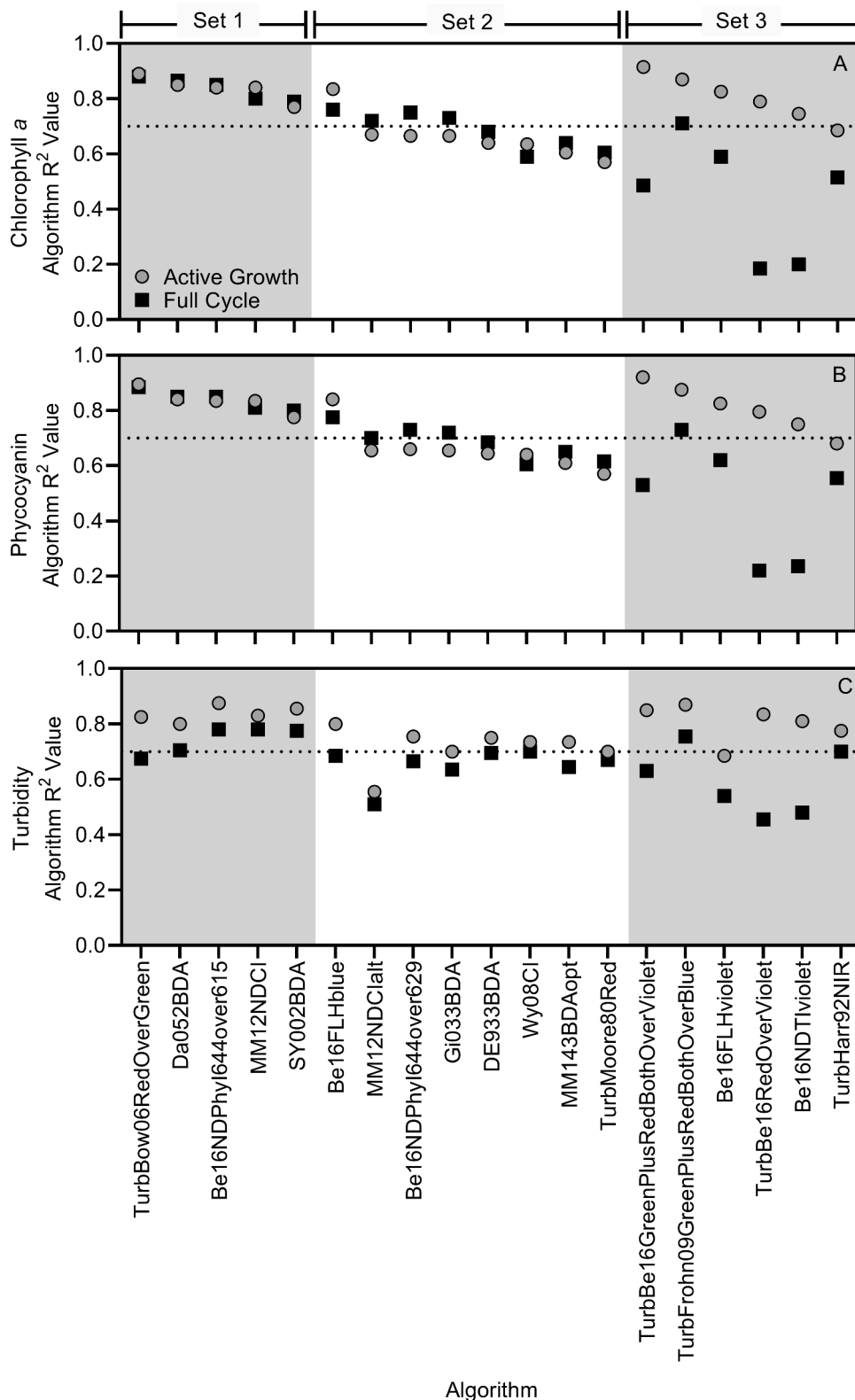

Figure 8. Comparison of average R^2 values for each algorithm with algorithm R^2 values above 0.70 (horizontal dotted line) for at least one water quality indicator: chlorophyll *a* (A), phycocyanin (B) or turbidity (C), and/or growth phase (Active Growth; gray circles, Full Cycle: black squares), arranged by degree of separation according to chlorophyll *a* values, where Set 1 indicates those with < 5% separation, Set 2 indicates those with moderate (5% ≤ 15% difference in R^2 values for chlorophyll *a*) differences in average algorithm performance by growth phase, and Set 3 signifies major growth phase differences in algorithm performance (> 20% difference in R^2 values for chlorophyll *a*).

between growth phases. Of the five algorithms in Set 1 that performed well for chlorophyll *a* and phycocyanin, none of the algorithms had < 5% difference in algorithm R^2 values between growth phases for turbidity. For turbidity, the lowest observed difference between growth phases was 6%, seen for the MM12NDCI algorithm (Fig. 8). For turbidity, all other algorithms in Set 1 had growth phase differences in algorithm R^2 values between 10% and 20%, additionally one of five had R^2 values for the Full Cycle group below 0.70. Additionally, for turbidity the Active Growth group had consistently higher average R^2 values across all algorithms in Set 1 (Fig. 8).

In Set 2 for chlorophyll *a* and phycocyanin, average R^2 values had deviations between growth phases ranging from 5% to 12% (Fig. 8). One of the eight algorithms (Be16FLHblue) had R^2 values above 0.70 for chlorophyll *a* and phycocyanin for both growth phases. The next three algorithms in Set 2 (MM12NDCIalt, Be16Phy2BDA644over629, and Gi033BDA) had R^2 values above 0.70 in the Full Cycle but below 0.70 in Active Growth for cyanobacteria pigments. The last four algorithms in Set 2 (DE933BDA, Wy08CI, MM143BDAopt, and TurbMoore80Red), had algorithm R^2 values below 0.70 for both growth phases for chlorophyll *a* and phycocyanin. In Set 2 for turbidity, in the Active Growth group all but one algorithm (MM12NDCIalt at R^2=0.56) had R^2 values above 0.70 where all algorithms in the Full Cycle had R^2 values at or below 0.70, again suggesting poor alignment of R^2 values between growth phases for this water quality indicator. The higher algorithm performance in the Active Growth group was consistent between Set 1 and 2 for turbidity.

In Set 3, the Active Growth group had algorithm R^2 values that were consistently greater than the Full Cycle for all water quality indicators with growth phase deviations ranging from 21% to 125% for chlorophyll *a*, 18% to 114% for phycocyanin, and 10% to 59% for turbidity (Fig. 8). Five of the six algorithms in Set 3 had Active Growth R^2 values above 0.70 for chlorophyll *a* and phycocyanin, and all but one (TurbFrohn09GreenPlusRedBothOverBlue) of the Full Cycle R^2 values were below 0.70. For turbidity, all but one algorithm (Be16FLHviolet at R^2=0.68) had R^2 values above 0.70 for Active Growth and all but two algorithms (TurbFrohn09GreenPlusRedBothOverBlue at R^2=0.76) had R^2 values at or below 0.70 for the Full Cycle.

Across all Sets, algorithms that included a blue or violet spectral band (400 nm - 480 nm), including TurbBe16GreenPlusRedBothOverViolet, TurbFrohn09GreenPlusRedBothOverBlue, TurbBe16RedOverViolet, Be16 NDTviolet, Be16FLHviolet, and Be16FLHblue, in general had the largest (> 15%) disagreement between growth phases across each of the water quality indicators (Fig. 8). Where these algorithms performed well on the Active Growth group with R^2 values all above 0.70 but performed poorly

on the Full Cycle group with R^2 values all below 0.70 across all water quality indicators. It is clear from Set 3 that depending on the algorithm, algorithm R^2 values can be heavily impacted by algal growth stage and overall physiological state.

3.6. Algorithm Error

In Set 1, four of the five algorithms had errors ≤ 30% across all water quality indicators and growth phases, including TurbBow06RedOverGreen (17%-30%), Da052BDA (19%-28%), Be16NDPhyI644over615 (20%-29%), and MM12NDCI (21%-25%) (Tbl. 5). In Set 2, only one algorithm had errors ≤ 30% for all water quality indicators and growth phases namely, Be16FLHblue (22%-29%) (Tbl. 5). In Set 3, all algorithms had > 30% error for at least one water quality indicator/growth phase (Tbl. 5). Additionally, MAPEs in the Full Cycle were consistently greater than Active Growth for all water quality indicators in Set 3, comparable to the greater differences in algorithm R^2 values for this set (Fig. 8).

4. Discussion

Due to the operational flexibility afforded by UAS platforms and the spectral resolution of hyperspectral sensors, these technologies were combined to explore and evaluate the complexities of detecting cyano-HABs in a controlled environment to help bridge the gap between laboratory and field studies. In this study, the progression of a *Microcystis* sp. bloom in controlled mesocosms was monitored over an 11-day period using multiple methods, including laboratory grab samples, *in-situ* field probes, and a UAS hyperspectral sensor. More specifically, the methods were statistically compared to illustrate differences for measuring HAB water quality indicators (chlorophyll *a*, phycocyanin and turbidity) across bloom physiological state (algal growth stages/life cycle) using spectrally-derived water quality algorithms.

4.1. Water quality indicators as estimates of cyanobacteria biomass

There are well known technological interferences and limitations owing to 1) spectral variability in detectors, 2) upper and lower working limits, and 3) sample heterogeneity, related to cell volume/colony size that can impact the accuracy of *in situ* field probes, specifically for cyanobacteria (reviewed in Bertone et al., 2018; Hodges et al., 2017). The impact of *in situ* probe performance, commonly used to validate remote sensing methods, could therefore, potentially bias biomass estimates and impact routine monitoring programs and/or regional

Table 5
Mean absolute percentage error (MAPE) for top algorithms for all water quality indicators (averaged over lab and field methods).

Set	Algorithm	Chlorophyll *a*		Phycocyanin		Turbidity	
		Active	Full	Active	Full	Active	Full
1	TurbBow06RedOverGreen	17%	17%	20%	19%	23%	30%
	Da052BDA	23%	19%	27%	22%	26%	28%
	Be16NDPhyI644over615	26%	21%	29%	24%	20%	24%
	MM12NDCI	21%	22%	25%	23%	22%	23%
	SY002BDA	33%	26%	38%	29%	23%	26%
2	Be16FLHblue	25%	25%	28%	27%	22%	29%
	MM12NDCIalt	38%	29%	46%	34%	39%	33%
	Be16NDPhyI644over629	38%	28%	42%	31%	28%	28%
	Gi033BDA	31%	24%	37%	28%	31%	31%
	DE933BDA	39%	30%	45%	34%	29%	30%
	Wy08CI	42%	38%	48%	40%	29%	28%
	MM143BDAopt	37%	32%	43%	34%	29%	31%
	TurbMoore80Red	44%	34%	50%	38%	33%	32%
3	TurbBe16GreenPlusRedBothOverViolet	16%	39%	18%	41%	20%	28%
	TurbFrohn09GreenPlusRedBothOverBlue	24%	29%	26%	31%	19%	25%
	Be16FLHviolet	28%	33%	32%	36%	32%	30%
	TurbBe16RedOverViolet	26%	51%	29%	55%	22%	36%
	Be16NDTIviolet	31%	51%	34%	55%	25%	35%
	TurbHarr92NIR	34%	38%	40%	40%	29%	29%

forecasts. For example, some probes are developed with wide bandpass filters for chlorophyll *a* and phycocyanin to account for spectral variability owing to algal physiological changes associated with environmental factors. However, these wider filters can lead to a greater occurrence of false positives owing to overlapping chlorophyll *a* and phycocyanin emission spectra and turbidity interferences in phycocyanin estimates, among others (discussed in Bertone et al., 2018).

Many studies have shown that field probes for chlorophyll *a* and phycocyanin correlate well with cyanobacteria biomass indicators in laboratory experiments including cell counts and/or corresponding *in vivo* (absorbance-based) or *in vitro* (extracted) pigments (Bastien et al., 2011; Brient et al., 2008; Gregor and Marsalek, 2004). For example, Bertone et al. (2019) compared *in vivo* pigment fluorescence from an EXO2 sonde, similar to the one used in this study, to laboratory spectrophotometer measurements (absorbance based) across three cyanobacteria species in monoculture. Bertone et al. (2019), found a high correlation (R^2-values above 0.93) between endpoints for *Sphaerospermopsis* sp. and *Aphanocapsa* sp., but a low correlation between endpoints for *Raphidiopsis raciborskii* for phycocyanin. They also found high correlations (R^2-values > 0.94) between endpoints for all three species for *in vivo* chlorophyll *a*. The authors concluded that while correlations between sensors/endpoints may be high, it is also species-specific, and species-level pigmentation differences have the potential to over or underestimate cyanobacterial biomass in *in-situ* field sensors (Bertone et al., 2019). However, few studies to date have compared *in vivo* fluorescence-based laboratory methods to field probes as estimates of algal biomass, especially with respect to remote sensing data. This is important as fluorometric endpoints are known to be more sensitive than spectrophotometric endpoints, though *in vivo* measures tend to be less precise than *in vitro* measures (discussed in Bertone et al. 2018).

Instrumentation variations in measurement wavelengths, bandwidths, and limits of detection have the potential to influence algorithm performance, which is directly related to the band math used in each algorithm and can thus impact biomass estimations from imagery. For example, Hodges et al. (2017) tested five *in situ* phycocyanin probes and found dramatically different working upper limits between instruments ranging from 1,200 to greater than 12,000 µg•L^{-1}, highlighting the importance of understanding the limitations and appropriateness of available sensors. In this study, in general, there was strong agreement between methods (Lab and Field) for all water quality indicators independent of growth phase with regression R^2-values above 0.70 for MAPEs and 0.86 for algorithm R^2 values (Fig. 5, Tbl. 4). However, for MAPEs regression lines for chlorophyll *a* and turbidity statistically differed from a hypothetical slope of zero. Moreover, regression lines for all water quality indicators differed from a hypothetical slope of zero for algorithm R^2 values (Tbl. 4). Collectively, this indicates potential methodological bias, particularly at higher errors and lower algorithm R^2 values. However, it is unclear if the potential methodological bias would have a measurable impact on downstream analyses. It is also unlikely that this methodological bias in algorithm performance would exceed the benefits and common practice of using *in situ* probes to monitor biomass. For instance, the affordability and near real-time results of field probes outweigh the time constraints and high costs associated with grab samples requiring laboratory analysis (Beck et al., 2016; Beck et al., 2017; Beck et al., 2019); nevertheless, it is important to understand the limitations of this instrumentation.

Measuring methods (e.g. absorbance, fluorescence, nephelometry) may also vary by instrumentation and can also dramatically influence downstream results. For example, turbidity measures had lower regression R^2 values for both MAPEs and algorithm R^2 values at 0.70 and 0.86, independent of growth phase. The low R^2-value reported likely has to do with the different measurement wavelengths and endpoints (scattering vs absorbance) where the Lab method measured turbidity via absorbance at 750 nm and the Field method measured turbidity through light scattering or nephelometry at 860 nm. The algorithms used here

were expected to detect biomass based on both the absorption and backscattering from phytoplankton cells, namely algal pigments. However, nephelometric turbidity measures only depend on scattering properties. These types of broad water quality sensors are designed to encapsulate a range of pigments and organic/inorganic particulate material (refractive index) and take into account the shape and size of particulates. Given that most of the turbidity found in the experimental tanks were derived from the algal pigments: chlorophyll *a* and phycocyanin, it makes sense that during Active Growth, algorithms performed reasonably well for turbidity with 15 of the 19 high performing algorithms having R^2 values above 0.70 (Fig. 5, Fig. 8). However, in the Full Cycle there was likely algal turnover during bloom senescence that could result in increased cellular debris and backscattering in the water column; thus, it is reasonable that algorithm R^2 values decreased in this group where only five of the 19 high performing algorithms had R^2 values above 0.70. It is therefore important to understand the limitations of the *in-situ* probe for each remote sensing study and to recognize the impact of the site environment and algal physiological state on data accuracy and reliability. Furthermore, it is important to note that algorithm performance may also be impacted by the physical conditions of the water as they relate to algal physiological state, which are important considerations when designing field campaigns and purchasing field instrumentation.

4.2. Algorithm Performance

In this investigation, algorithm performance was used as a metric to evaluate the consistency of traditional spectrally-derived algorithms across data collection methodologies and algal growth phases. It is important to note that the suite of algorithms utilized in this study were primarily developed for and commonly used with satellite platforms. Algorithms use unique band math associated with water quality absorbance features, typically derived from satellite multispectral imagery, but in this case, derived from UAS hyperspectral imagery to help bridge the gap between ground sampling measurements and remote sensing technology.

The potential bias from physiological changes in cyanobacteria have great implications in the field of remote sensing, in which growth phase bias in field studies can impact the accuracy and precision of satellite-based algorithms, particularly during single snapshots in time. The goal was to identify a suite of algorithms that performed comparably for each of the three water quality indicators as determined by algorithm R^2 values and relative error. Benchmark criteria were that algorithm R^2 values must be above 0.70, have < 15% deviation between growth phases (Active Growth vs Full Cycle), and have $\leq$ 30% error across all water quality indicators. A total of three out of 41 algorithms met these criteria including: Da052BDA, Be16NDPhyl644over615, and MM12NDCI (Fig. 8, Tbl. 5). However, if turbidity is excluded the number of algorithms meeting the benchmark criteria increases to five for chlorophyll *a* and phycocyanin, including TurbBow06RedOverGreen and BeFLHblue (Fig. 8, Tbl. 5). These algorithms appear to generally be effective for modeling estimates of algal biomass given their high degree of portability across these common water quality indicators.

Of additional note was the growth phase variation in performance of algorithms that had blue or violet wavebands (e.g. ∼ 400 nm – 480 nm) for all water quality indicators (Fig. 8). For example, TurbBe16-GreenPlusRedBothOverViolet was actually one of the highest performing algorithms in the Active Growth group for all indicators (R^2 values $\geq$ 0.85), but performance dropped well below an R^2-value of 0.70 (R^2 values $\leq$ 0.63) and increased MAPE by up to 26% in the Full Cycle group (Fig. 8, Tbl. 5). The exact mechanism(s) for this decreased algorithm performance was not confirmed in this study, however it is possible that algal physiology may have a wider impact on algorithms that have blue or violet wavelengths (∼ 400 nm – 480 nm).

5. Conclusion

Ground sampling and new remote sensing technologies can provide powerful approaches for bloom monitoring. This study highlights the importance of co-validating sensor technologies with appropriate ground sampling methods to gain foundational knowledge before transitioning new technologies to large-scale research efforts or operational use. Controlled studies like this one help build consistency across sampling tools/approaches and demonstrate the utility of new technologies for bloom monitoring to advance the state of science. However, more research is needed to evaluate how algorithms and water quality indicators perform in the field under various bloom consortia, cell densities, physiological states, and water clarity conditions, especially with respect to algorithms having blue/violet wavebands which particularly struggled with growth phase changes. It's also important to note that this study utilized algorithms developed for spectrally and spatially coarser multispectral satellite sensors; thus, their application to higher resolution sensors may yield variable results. Yet, studies that continue to bridge technological gaps have implications for improving forecasting and monitoring efforts by building confidence in the accuracy and precision of available ground-validated spectrally-derived algorithms, their utility for detecting cyanoHAB events, and portability to other remote-sensing platforms.

6. Disclaimer

Views, opinions and/or findings contained herein are those of the authors and should not be construed as an Official Department of the Army or National Oceanic and Atmospheric Administration position or decision unless so designated by other official documentation.

Author Statement

Kaytee Pokrzywinski: Conceived of the presented study, developed the theory and performed computations, verified analytical methods, conducted formal analysis of data/data curation, preparation of figures, supervised findings of the work, managed and coordinated project, acquired financial support for the project, and discussed the results and took the lead in writing the final manuscript. Richard Johansen: Assisted with the development of the study methodology, conducted formal analyses, prepared tables and figures, and co-led the writing and editing of the final manuscript. Molly Reif: Assisted with project management and coordination, helped with data evaluation and preparing data for analysis, and provided critical manuscript review and editing. Scott Bourne: Assisted with the unmanned aircraft systems (UAS) and ground based hyperspectral field data collection. Preformed Radiometric corrections and georectification of all hyperspectral data. Contributed to manuscript writing and editing. Shea Hammond: Managed unmanned aircraft systems field data collection, assisted with field data preparation for analysis, and contributed to manuscript writing and editing. Brianna Fernando: Assisted in analyzing the data through computational analysis, created figures, and contributed to manuscript editing.

Declaration of Competing Interest

The authors declare that they have no known competing financial interests or personal relationships that could have appeared to influence the work reported in this paper.

Acknowledgements

Supplementary materials

Supplementary material associated with this article can be found, in the online version, at doi:10.1016/j.hal.2022.102268.

References

Amin, R., Zhou, J., Gilerson, A., Gross, B., Moshary, F., Ahmed, S., 2009. Novel optical techniques for detecting and classifying toxic dinoflagellate Karenia brevis blooms using satellite imagery. Optics Express 17 (11), 9126.

Andersen, R.A., 2005. Algal Culturing Techniques, first ed. Burlington, Massachusetts.

Bastien, C., Cardin, R., Veilleux, É., Deblois, C., Warren, A., Laurion, I., 2011. Performance evaluation of phycocyanin probes for the monitoring of cyanobacteria. Journal of Environmental Monitoring 13 (1), 110–118.

Bertone, E., Burford, M.A., Hamilton, D.P., 2018. Fluorescence probes for real-time remote cyanobacteria monitoring: a review of challenges and opportunities. Water Research 141, 152–162.

Bertone, E., Chuang, A., Burford, M.A., Hamilton, D.P., 2019. In-situ fluorescence monitoring of cyanobacteria: Laboratory-based quantification of species-specific measurement activity. Harmful Algae 87, 10165.

Beck, R., Xu, M., Zhan, S., Liu, H., Johansen, R., Tong, S., Yang, B., et al., 2017. Comparison of satellite reflectance algorithms for estimating phycocyanin values and cyanobacterial total biovolume in a temperate reservoir using coincident hyperspectral aircraft imagery and dense coincident surface observations. Remote Sensing 9 (6), 538.

Beck, R., Xu, M., Zhan, S., Johansen, R., Liu, H., Tong, S., Yang, B…., Huang, Y., 2019. Comparison of satellite reflectance algorithms for estimating turbidity and cyanobacterial concentrations in productive freshwaters using hyperspectral aircraft imagery and dense coincident surface observations. Journal of Great Lakes Research 45 (3), 413–433.

Beck, R., Zhan, S., Liu, H., Tong, S., Yang, B., Xu, M., Ye, S., et al., 2016. Comparison of satellite reflectance algorithms for estimating chlorophyll-a in a temperate reservoir using coincident hyperspectral aircraft imagery and dense coincident surface observations. Remote Sensing of Environment 178, 15–30.

Brient, L., Lengronne, M., Bertrand, E., Rolland, D., Sipel, A., Steinmann, D., Baudin, I., Legeas, M., Le Rouzic, B., Bormans, M., 2008. A phycocyanin probe as a tool for monitoring cyanobacteria in freshwater bodies. Journal of Environmental Monitoring 10 (2), 248–255.

Cillero Castro, C., Domínguez Gómez, J.A., Delgado Martín, J., Hinojo Sánchez, B.A., Cereijo Arango, J.L., Cheda Tuya, F.A., Díaz-Varela, R., 2020. An UAV and satellite multispectral data approach to monitor water quality in small reservoirs. Remote Sensing. 12, 1514. In: Canty, A., Ripley, B., 2020. boot: Bootstrap R (S-Plus) Functions. R package version 1.3-25.

Davis, C., Bissett, W., 2007. Characterization of a harmful algal bloom in Monterey Bay, CA using airborne hyperspectral imagery. Fourier Transform Spectroscopy/ Hyperspectral Imaging and Sounding of the Environment, OSA Technical Digest Series (CD). Optical Society of America paper HMC4.

Dekker, A.G., 1993. Detection of optical water quality parameters for eutrophic waters by high resolution remote sensing. Free University Amsterdam.

Graham, J.L., 2006. Harmful algal blooms. USGS Fact Sheet 2006–3147.

Gregor, J., Maršálek, B., 2004. Freshwater phytoplankton quantification by chlorophyll a: A comparative study of in vitro, in vivo and in situ methods. Water Research 38 (3), 517–522.

Gustavs, L., Schumann, R., Eggert, A., Karsten, U., 2009. In vivo growth fluorometry: Accuracy and limits of microalgal growth rate measurements in ecophysiological investigations. Aquatic Microbial Ecology 55, 95–104.

Havens, K.E., 2008. Chapter 33: Cyanobacteria blooms: effects on aquatic ecosystems. In: Hudnell, H.K. (Ed.), Cyanobacterial Harmful Algal Blooms: State of the Science and Research Needs. Springer Science + Business Media, LLC.

Hodges, C.M., Wood, S.A., Puddick, J., McBride, C.G., Hamilton, D.P., 2018. Sensor manufacturer, temperature, and cyanobacteria morphology affect phycocyanin fluorescence measurements. Environmental Science and Pollution Research 25, 1079–1088.

Hruska, R., Mitchell, J., Anderson, M., Glenn, N.N., 2012. Radiometric and geometric analysis of hyperspectral imagery acquired from an unmanned aerial vehicle. Remote Sensing 4 (9), 2736–2752.

International Ocean-Colour Coordinating Group (IOCCG), 2019. Uncertainties in Ocean Colour Remote Sensing. In: Mélin, F. (Ed.), IOCCG Report Series, No. 18. International Ocean Colour Coordinating Group, Dartmouth, Canada.

Johansen, R., Reif, M., Emery, E., Nowosad, J., Beck, R., Xu, M., Liu, H., 2019. waterquality: An open-source R package for the detection and quantification of cyanobacterial harmful algal blooms and water quality. Engineer Research and Development Center (U.S.) TR-19-20.

Kloiber, S.M., Brezonik, P.L., Olmanson, L.G., Bauer, M.E., 2002. A procedure for regional lake water clarity assessment using landsat multispectral data. Remote Sensing of Environment 82 (1), 38–47.

Lekki, J., Ruberg, S., Binding, C., Anderson, R., Woude, V., 2019. A. Airborne hyperspectral and satellite imaging of harmful algal blooms in the Great Lakes Region: Successes in sensing algal blooms. Journal of Great Lakes Research 45 (3), 405–412.

Linkov, I., Satterstrom, F.K., Loney, D., Steevens, J.A., 2009. The impact of harmful algal blooms on USACE operations:" Fort Belvoir. Defense Technical Information Center, VA. https://doi.org/10.21236/ada494537.

MacIntyre, H.L., Cullen, J.J., 2005. Using cultures to investigate the physiological ecology of microalgae. In: Andersen, R.A. (Ed.), Algal Culturing Techniques. Elsevier Academic Press, Massachusetts, pp. 287–326.

Maxwell, K., Johnson, G.N., 2000. Chlorophyll fluorescence - a practical guide. Journal of Experimental Botany 51 (345), 659–668.

Mishra, S., Mishra, D.R., 2014. A novel remote sensing algorithm to quantify phycocyanin in cyanobacterial algal blooms. Environmental Research Letters 9 (11), 114003.

Mishra, S., Mishra, D., Schluchter, W., 2009. A novel algorithm for predicting phycocyanin concentrations in cyanobacteria: A proximal hyperspectral remote sensing approach. Remote Sensing 1 (4), 758–775.

Mishra, S., Stumpf, R.P., Schaeffer, B.A., Werdell, P.J., Loftin, K.A., Meredith, A., 2019. Measurement of cyanobacterial bloom magnitude using satellite remote sensing. Scientific Reports 9, 18310.

Ni, Z., Lu, Q., Huo, H., Zhang, H., 2019. Estimation of chlorophyll fluorescence at different scales: A review. Sensors 19, 3000.

Paerl, H.W., Fulton, R.S., Moisander, P.H., Dyble, J., 2001. Harmful freshwater algal blooms, With an Emphasis on Cyanobacteria. The Scientific World Journal 1, 76–113.

Pokrzywinski, K., Place, A.R., Warner, M.E., Coyne, K.J., 2012. Investigation of the algicidal exudate produced by Shewanella sp. IRI-160 and its effects on dinoflagellates. Harmful Algae 12, 23–29.

Core Team, R, 2017. R: A language and environment for statistical computing. R Foundation for Statistical Computing, Vienna, Austria https://www.R-project. org/.

Randolph, K., Wilson, J., Tedesco, L., Li, L., Pascual, D.L., Soyeux, E., 2008. Hyperspectral remote sensing of cyanobacteria in turbid productive water using optically active pigments, chlorophyll a and phycocyanin. Remote Sensing of Environment 112 (11), 4009–4019.

Ritchie, J.C., Zimba, P.V., Everitt, J.H., 2003. Remote sensing techniques to assess water quality. Photogrammetric Engineering & Remote Sensing 69 (6), 695–704.

Schalles, J., Yacobi, Y., 2000. Remote detection and seasonal patterns of phycocyanin, carotenoid and chlorophyll pigments in eutrophic waters. Archiv. Fur. Hydrobiologie. Special Issues Advances in Limnology. 55, 153–168.

Shen, L., Xu, H., Guo, X., 2012. Satellite remote sensing of harmful algal blooms (HABs) and a potential synthesized framework. Sensors 12 (6), 7778–7803.

Simis, S., Steef, G.H., Peters, W.M., Gons, H.J., 2005. Remote sensing of the cyanobacterial pigment phycocyanin in turbid inland water. Limnology and Oceanography 50 (1), 237–245.

Stumpf, R.P., Davis, T.W., Wynne, T.T., Graham, J.L., Loftin, K.A., Johengen, T.H., Gossiaux, D., Palladino, D., Burtner, A., 2016. Challenges for mapping cyanotoxin patterns from remote sensing of cyanobacteria. Harmful Algae 54, 160–173.

Takahashi, T., 2019. Routine management of microalgae using autofluorescence from chlorophyll. Molecules 24 (24), 4441.

Wang, L., Fan, D., Chen, W., Terentjev, E.M., 2015. Bacterial growth, detachment and cell size control on polyethylene terephthalate surfaces. Scientific Reports. 5, 15159.

Wood, A.M., Everroad, R.C., Wingard, L.M., 2005. Measuring growth rates in microalgal cultures. In: Andersen, R.A. (Ed.), Algal Culturing Techniques. Elsevier Academic Press, Massachusetts, pp. 269–285.

Wynne, T.T., Stumpf, R.P., Tomlinson, M.C., Warner, R.A., Tester, P.A., Dyble, J., Fahnenstiel, G.L., 2008. Relating spectral shape to cyanobacterial blooms in the Laurentian Great Lakes. International Journal of Remote Sensing 29 (12), 3665–3672.

YSI, 2020. EXO User Manual: ADVANCED WATER QUALITY MONITORING PLATFORM. Xylem Inc, Yellow Springs, OH.